

Identification of fibrillogenic regions in human triosephosphate isomerase

Edson N Carcamo-Noriega, Gloria Saab-Rincon

Background. Amyloid secondary structure relies on the intermolecular assembly of polypeptide chains through main-chain interaction. According to this, all proteins have the potential to form amyloid structure, nevertheless, in nature only few proteins aggregates into toxic or functional amyloids. Structural characteristics differ greatly among amyloid-former proteins reported, so it has been difficult to link the fibrillogenic propensity with structural topology. However, there are ubiquitous topologies not represented in the amyloidome that could be considered as amyloid-resistant attributable to structural features, such is the case of TIM barrel topology.

Methods. This work was aimed to study the fibrillogenic propensity of human triosephosphate isomerase (HsTPI) as a model of TIM barrels. In order to do so, aggregation of HsTPI was evaluated under native-like and destabilizing conditions. Fibrillogenic regions were identified by bioinformatics approaches, and further tested by protein fragmentation and peptide aggregation.

Results. We identified four fibrillogenic regions in the HsTPI corresponding to the $\beta 3$, $\beta 6$, $\beta 7$ y $\alpha 8$ of the TIM barrel. From these, the $\beta 3$ -strand region (residues 59-66) was highly fibrillogenic. In aggregation assays, HsTPI under native-like conditions led to amorphous assemblies while in partially denaturing conditions (urea 3.2 M) formed more structured aggregates. This slightly structured aggregates exhibited residual cross- β structure, as demonstrated by the recognition of the WO1 antibody and ATR-FTIR analysis.

Discussion. Despite the fibrillogenic regions present in HsTPI, the enzyme maintained under strongly native-favoring conditions displayed low fibrillogenic propensity. This amyloid-resistance can be attributed to the three-dimensional arrangement of the protein, where β -strands, susceptible to aggregation, are protected in the core of the molecule.

1 **Title:** Identification of Fibrillogenic Regions in Human Triosephosphate Isomerase.

2 **Author names and affiliations:** Edson Norberto Carcamo-Noriega¹, Gloria Saab-
3 Rincon¹.

4 ¹Departamento de Ingeniería Celular y Biocatálisis, Instituto de Biotecnología, Universidad
5 Nacional Autónoma de México.

6 **Corresponding author:** Gloria Saab-Rincon, Departamento de Ingeniería Celular y
7 Biocatálisis, Instituto de Biotecnología, Universidad Nacional Autónoma de México, Av.
8 Universidad No. 2001, Col. Chamilpa C.P. 62210, Cuernavaca, Morelos, México. Tel.: +52
9 (777) 329-1640; Email: gsaab@ibt.unam.mx

1. Abstract

Background. Amyloid secondary structure relies on the intermolecular assembly of polypeptide chains through main-chain interaction. According to this, all proteins have the potential to form amyloid structure, nevertheless, in nature only few proteins aggregates into toxic or functional amyloids. Structural characteristics differ greatly among amyloid-former proteins reported, so it has been difficult to link the fibrillogenic propensity with structural topology. However, there are ubiquitous topologies not represented in the amyloidome that could be considered as amyloid-resistant attributable to structural features, such is the case of TIM barrel topology.

Methods. This work was aimed to study the fibrillogenic propensity of human triosephosphate isomerase (HsTPI) as a model of TIM barrels. In order to do so, aggregation of HsTPI was evaluated under native-like and destabilizing conditions. Fibrillogenic regions were identified by bioinformatics approaches, and further tested by protein fragmentation and peptide aggregation.

Results. We identified four fibrillogenic regions in the HsTPI corresponding to the $\beta 3$, $\beta 6$, $\beta 7$ y $\alpha 8$ of the TIM barrel. From these, the $\beta 3$ -strand region (residues 59-66) was highly fibrillogenic. In aggregation assays, HsTPI under native-like conditions led to amorphous assemblies while in partially denaturing conditions (urea 3.2 M) formed more structured aggregates. This slightly structured aggregates exhibited residual cross- β structure, as demonstrated by the recognition of the WO1 antibody and ATR-FTIR analysis.

Discussion. Despite the fibrillogenic regions present in HsTPI, the enzyme maintained under strongly native-favoring conditions displayed low fibrillogenic propensity. This amyloid-resistance can be attributed to the three-dimensional arrangement of the protein, where β -strands, susceptible to aggregation, are protected in the core of the molecule.

34 Destabilization of the protein structure may expose inner regions promoting β -aggregation.
 35 However, the highly hydrophobic nature of the protein core favors the formation of
 36 hydrophobic disordered aggregates. This pathway seems to be kinetically favored over the
 37 thermodynamically more stable fibril aggregation pathway.

38 **Keywords:** Fibrillogenesis; amyloid; aggregation; Triosephosphate isomerase; Cross- β

2. Introduction

The conversion of native soluble proteins into highly structured insoluble fibrillar assemblies is associated with several degenerative pathologies, such as Alzheimer's disease, Huntington's disease and Parkinson's disease, among others¹. Currently, more than 30 different proteins are involved in amyloid processes that differ in their sequence, topology, size and function but share similar structural features in the fibrils formed. A common unit of the cross- β spine structure is conserved in fibrillar assemblies, where β -strands stack perpendicular to the fiber axis to form β -sheets that grow along the fibril axis²⁻⁴. Several fibrillogenesis mechanism models have been proposed based on kinetic, structural and morphological data⁵. These mechanisms differ from each other by: i) the number of aggregation pathways, ii) number of steps (conformational and oligomeric states of the protein) and iii) the cooperativity of amyloid assembly⁶⁻¹².

Regardless the mechanism followed, amyloid fibril formation always relies on the intermolecular interactions of the polypeptide main chain. Therefore, all polypeptide chains have the potential to form β -aggregates. However, not all proteins aggregate into cross- β structures in the physiological environment¹³. To observe protein aggregation, the native state must usually be destabilized to expose aggregation-prone regions². It is clear that some sequences are more prone to form cross- β structures than others¹⁴. Some experimental and computational studies have identified the inherent properties of the sequence, including the net charge, length, hydrophobicity and secondary structure propensities, as determinants of aggregation¹⁵⁻¹⁷. Based on experimental evidence, several informatics approaches have been developed to identify aggregation-prone regions that could allow us to predict protein aggregation propensity.

These aggregation-prone regions are present in a large number of proteins and, in some cases, play a key role in the function or folding of the protein and, therefore, cannot be eliminated. However, evolution has developed protective mechanisms, such as improving solubility, steric hindrance and conformational restriction, to avoid the exposure of aggregation-prone regions^{18,19}. It is clear that most of the protective mechanisms that evolved are based on increasing the stability of the native state of the protein, suggesting that topologies with higher stabilities are less susceptible to amyloid aggregation¹³. Thus, this trait can be selected during evolution, which may explain the rather limited number of folds observed in nature^{20,21}.

A scaffold that has been recursively recruited during evolution is the TIM barrel (β/α)₈²². So far, there are no reports of any TIM barrel forming fibrillar aggregates. Nevertheless, there is some evidence that links triosephosphate isomerase (TPI) with amyloid aggregation. In 1999, Contreras et al., found a segment (residues 186-218) from *Escherichia coli* TPI that shares 20 % identity with the amyloid β -peptide²³. When investigated, this fragment was able to assemble into amyloid-like fibrils with affinity to Congo red. In another work, Guix et al., found high levels of a nitrated variant of TPI (nitro-TPI) that was induced by amyloid β -peptide depositions in the brain tissues of Alzheimer's disease patients²⁴. Aggregation of *in vitro* nitrated rabbit TPI formed large β -aggregates with amyloid-like properties that were able to induce aggregation of the Tau protein. These data indicate a fibrillogenic potential in TIM barrels, moreover in human triosephosphate isomerase (HsTPI) with interest in the physiopathology of Alzheimer's disease. Therefore we considered imperative to evaluate the *in vitro* propensity of HsTPI to aggregate into fibril conformation and search for fibrillogenic regions in its sequence.

3. Materials and methods

3.1. Materials.

All peptides were synthesized by Liquid Phase Peptide Synthesis (LPPS) without N- or C-terminal modifications by GenScript USA Inc. (Figure 3B). The WO1 antibody was generously donated by Dr. Ronald Wetzel from the Department of Structural Biology of the University of Pittsburgh. Hen egg-white lysozyme (HEWL) and all other reagents were purchased from Sigma-Aldrich Co (St. Louis, MO, USA).

3.2. Expression and purification of HsTPI.

The vector pET3a-HsTPI was kindly donated by Dr. Gomez Poyou (IFC-UNAM). This vector encodes the sequence of the wild-type HsTPI with a His-tag at the N-terminus followed by a TEV protease recognition sequence. The plasmid was transformed into the *E. coli* BL21-Gold(DE3) strain. Transformed cells were grown in LB medium containing ampicillin at 37 °C until an absorbance of 0.6 at 600 nm was reached. Then, the expression of HsTPI was induced with IPTG at a final concentration of 0.2 mM. Incubation continued at 20 °C for 6 hrs. The cells were harvested and suspended in buffer A (20 mM sodium phosphate, 150 mM NaCl, pH 7.4). The cell suspension was sonicated (five times for 30 seconds) and centrifuged at 15,000 g for 30 minutes. The supernatant was loaded into a Ni-NTA agarose column. The resin was washed with 10 column volumes of buffer A containing 50 mM imidazole. HsTPI was then eluted with 300 mM imidazole in buffer A. The purified HsTPI was dialyzed against buffer A in order to eliminate the imidazole. The His₆X tag was cleaved using recombinant His-tagged TEV protease at a ratio of 1:50 (w/w) protease/HsTPI at 4 °C overnight. To remove the His-tagged TEV protease as well as any

undigested HsTPI, the mixture was loaded onto a Ni-NTA agarose column and washed with buffer A. The effluent from the column containing the cleaved HsTPI was recovered, precipitated with 75 % ammonium sulfate and stored at 4 °C. The protein concentration was determined by measuring the absorbance at 280 nm using an extinction coefficient of $\epsilon=33460 \text{ M}^{-1} \text{ cm}^{-1}$. The integrity of HsTPI was checked using a specific activity assay (data not shown).

3.3. Aggregation assays.

Aggregation assays were performed in 1.5-mL Eppendorf tubes containing 1 mL of 100 μM HsTPI previously dialyzed against buffer A supplemented with 0.2% of sodium azide. Aggregation was also performed under light denaturing conditions (3.2 M of urea in the same buffer). The tubes containing the enzyme were incubated in a thermomixer (Eppendorf, series: 22670000) at 37 °C and 600 rpm for one week. HsTPI aggregation was followed through time by Thioflavin T (ThT) fluorescence. To do so, protein samples (10 μL) were added to 140 μL of filtered 10 μM ThT in buffer A and the fluorescence emission intensity at 485 nm was recorded using black clear bottomed plates in a Tecan Safire multimode microplate reader at an excitation of 440 nm. After one week of incubation, the aggregates were recovered by centrifugation at 25,000 g for 1 hr. The aggregation kinetics were repeated three times with protein originating from different expression and purification batches. A 100 μM HEWL solution at pH 2.0 was used as positive control for fibril formation²⁵.

For peptide aggregation assays, desalted freeze-dried peptide was first dissolved. All but the $\beta 4$, $\beta 7$, and $\beta 8$ peptides were soluble in water. The $\beta 4$ and $\beta 7$ peptides were dissolved in 10% acetic acid while the $\beta 8$ peptide was dissolved in 100 mM of ammonium hydroxide.

After dissolving, peptide solutions were diluted with phosphate buffer, supplemented with 0.02% of sodium azide, to a final concentration of 50 μ M and the pH was adjusted to 7.4. Large particles were removed by micro filtration (0.45- μ m pore size). A 1 mL sample of each peptide solution in 1.5-mL Eppendorf tubes was sealed and incubated at 37 °C and 600 rpm for 3 weeks. The final ThT fluorescence intensity and green-birefringence with Congo red were measured.

3.4. Congo red birefringence.

Congo red binding analysis was conducted using a spectrophotometric assay. First, 10 μ L of an aggregate sample was added to 140 μ L of filtered 5 μ M Congo red in PBS. Congo red alone was used as a blank. The mixtures were incubated at room temperature for 30 minutes. Absorbance spectra from 400 nm to 700 nm were acquired on a Tecan Safire multimode microplate reader blanked with phosphate buffer. A maximum peak at 540 nm was indicative of red-green birefringence. A relative birefringence value was calculated using the ratio of absorbance at 540:490 nm, $b = (abs_{540nm} / abs_{490nm})$ based on previous reports^{26,27}.

3.5. Dot-blot assay.

To confirm cross- β structure in the aggregates, a dot-blot assay against the anti-cross- β WO1 antibody was performed. First, a 10 μ L sample was placed as a drop on a nitrocellulose membrane and allowed to dry. Non-specific binding sites were blocked with 5% (w/v) bovine serum albumin for 1 h at room temperature. The membrane was incubated for 1 hour with the WO1 antibody at a dilution of 1:8000 in phosphate buffer containing 0.05% (w/v) Tween 20 (T-PBS). The unbound primary antibody was washed three times

for 10 minutes with T-PBS. Then, the membrane was incubated for 1 h at room temperature with the secondary antibody (alkaline phosphates conjugated anti-mouse antibody; A3562-Sigma-Aldrich) using a dilution factor of 1:30,000 in T-PBS. The membrane was then washed 5 times with T-PBS for 10 minutes and revealed using the BCIP[®]/NBT-Blue Liquid Substrate System for Membranes for 10 minutes. The colorimetric reaction was stopped with MilliQ water.

3.6. Transmission electron microscopy (TEM).

The final aggregation products were placed on Formvar-coated 200 mesh copper grids for 1 minute. The grids were stained for 1 minute with 2% (w/v) uranyl acetate and then washed once with MilliQ water. The images were recorded on a ZEISS transmission electron microscope model LIBRA 120 operating at 120 kV.

3.7. Infrared spectroscopy .

Fourier-transform infrared (FTIR) spectra of HsTPI samples were recorded using a Perkin Elmer-Spectrum Rx1 spectrometer equipped with a zinc selenide (ZnSe) Attenuated total reflection (ATR) accessory. Sample treatment and data recording was carried out as previously described²⁸. A total of 256 accumulations at 1 cm⁻¹ of resolution were performed in the range of 1800-1500 cm⁻¹. Water-vapor spectrum was subtracted from all samples spectrum and then spectral intensities were normalized in the 1630 cm⁻¹ peak using the Spekwin32 software. Furthermore, raw spectra in amide I region (1700-1600 cm⁻¹) were analyzed by second-derivative with PeakFit 4.12 software using the Savitsky-Golay routine.

3.8. Cross-β region consensus prediction.

Potential fibrillogenic regions were predicted using HsTPI sequence (UniProt ID P60174-1). A consensus prediction was considered to be at least two sequence hits by any of the four different predictors used: FISH-AMYLOID, FOLD-AMYLOID, PASTA 2.0 and AMYLPRED 2. For all servers, the default parameters were used.

3.9. Acid hydrolysis of HsTPI.

The chemical cleavage reaction was carried out in 1.5-mL Eppendorf tubes. Ten mg of freeze dried HsTPI was dissolved in 1 mL of 10 mM HCl, 1 mM DTT, pH 2, and incubated at 65 °C for 8 hrs. After the incubation period, the reaction was cooled on ice and the hydrolysis pattern was analyzed by tricine SDS-PAGE stained with coomassie dye. The hydrolysis products were incubated at 37 °C and 600 rpm for 7 days. The resulting aggregates were washed five times with water and then disaggregated by mixing overnight at room temperature in 7.4 M guanidinium chloride (Gdm-HCl).

3.10. Mass spectroscopy analysis.

The dissolved aggregates were desalted using a SepPack C18 cartridge and analyzed by nanoliquid chromatography and tandem mass spectrometry (nLC-MS/MS) with collision-induced dissociation (CID) on a LTQ-Orbitrap Velos (Thermo-Fisher Co., San Jose, CA) integrated with EASY-nLC II (Thermo-Fisher Co. San Jose, CA). For reverse chromatography, a 25-cm analytical column (750-μm inner diameter) packed with C18 resin was used in a continuous flow of 400 nL/min in a 10-90% gradient of acetonitrile in 0.1% formic acid over 120 min. All spectra were acquired in a data-dependent mode at a resolution of 60000 with an m/z range of 300 to 1600. Ions with a charge of +2, +3 and +4 were isolated for fragmentation using a normalized collision energy value of 35 and an activation Q value of 0.25.

4. Results

4.1. HsTPI aggregation.

The β -aggregation propensity of HsTPI was evaluated by stirring while incubating it for 7 days at 37 °C under native-like conditions (HsTPI_n). Additionally the incubation was also carried out in 3.2 M of urea (HsTPI_{urea}), a condition slightly destabilizing but still at the native baseline of the unfolding transition^{29,30}. The kinetics of aggregation followed by ThT fluorescence showed no β -aggregation for HsTPI_n after 7 days of incubation. HsTPI_{urea}, on the other hand, aggregated into β -structures as indicated by the increase in ThT fluorescence intensity (Figure 1A). However the aggregation of HsTPI_{urea} did not follow a nucleated polymerization mechanism, like the one observed for lysozyme, a typical amyloid fibrillogenic protein. Instead, it was observed an extended log phase with the apparent lack of lag phase. Moreover, HsTPI_{urea} showed a very slow β -aggregation process, since ThT fluorescence did not reach a plateau phase after a week of incubation. Longer incubation was not possible due the loss of protein by adhesion to the tube and microbial contamination despite that sodium azide was added. The TEM images of the final aggregation products showed disordered aggregates with a fragmented appearance for HsTPI_n (Figure 1B). In the case of HsTPI_{urea} the aggregates formed displayed elongated structures co-aggregated with clusters of disordered aggregates that seem to be in an incomplete stage of the fibrillogenic pathway. This observation is in good agreement with the slow rate of β -aggregation as detected by ThT fluorescence.

ATR-FTIR was performed in order to evaluate the nature of the aggregates obtained after a week of incubation. The second-derivative of the IR spectrum of salted-out HsTPI shown two maximal peaks around 1655 and 1633 cm⁻¹ in the amide I region (Figure 2A).

These bands correspond to α -helix and β -sheet structures, respectively. This second-derivative ATR-FTIR spectrum was consistent with spectra of others (β/α)₈ barrel protein in H₂O³¹⁻³⁴. After one week incubation under native-favoring conditions, the secondary structure of HsTPI was virtually unchanged suggesting native-like aggregation. In contrast, HsTPI_{urea} showed an increase of β -structure (1624 cm⁻¹ band) upon aggregation. Some residual non- β secondary structure was maintained around 1656 cm⁻¹ indicating that β -aggregation was not complete. The additional β -structure formed upon aggregation was further confirmed as cross- β structure by dot-blot assay using the anti-cross- β WO1 antibody³⁵ (Figure 2B).

4.2. Fibrillogenic regions in HsTPI.

To identify the fibrillogenic regions in HsTPI, the primary structure was submitted to four servers that use different protein aggregation prediction algorithms: FISH-AMYLOID³⁶, FOLD-AMYLOID³⁷, AMYLPRED 2³⁸ and PASTA 2.0³⁹. The prediction algorithms were based on a database of fibrillogenic sequences of prions, disease-associated proteins and functional amyloid proteins¹⁶, as well as some physical-chemical principles, such as secondary structure propensity, hydrogen-bonding potential, chameleonic sequences (CS), fully buried regions and structure-breaker residues such as proline. The predictions reached a consensus for eight regions primarily located at the C-terminus half of the protein (Figure 3A). The sequences of these eight regions were selected to carry out aggregation assays (Figure 3B). These peptides comprise the three chameleonic regions: CS-1 (residues 141-153), CS-2 (residues 168-176) and CS-3 (residues 239-249); and five β -strand regions β 4 (residues 90-96), β 5 (residues 120-130), β 6 (residues 160-167), β 7 (residues 203-214) and β 8 (residues 226-236). Furthermore, the regions covering

the three non-recognized β -strand regions: β 1 (residues 6-14), β 2 (residues 37-45) and β 3 (residues 59-66), were also included for peptide aggregation assays due their inherent propensity to form parallel β -sheets and potential β -aggregation. To maximize the solubility of the synthetic peptides, extra native residues were added to the predicted regions as recommended by GenScript USA Inc (Supporting Information Table S1).

During the peptide aggregation assays, the β 3 peptide became turbid by the second day of incubation followed by the β 6, β 7 and CS-3 peptide, where turbidity appeared by the fifth day. Measurements of the final ThT fluorescence intensities at 485 nm were recorded for all of the samples. The β 3, β 6, β 7 and CS-3 peptide aggregates shown a clear increase in ThT fluorescence indicating β -aggregation (Figure 4A). The β 3 aggregates showed the highest ThT fluorescence intensity, indicating a major fibril formation for this sequence than for the β 6, β 7 and CS-3 sequences. In addition, aggregates of the β 3, β 6, β 7 and CS-3 peptides were tested in the spectrometric birefringence assays with Congo red⁴⁰. The four aggregates exhibited an amyloid indicative red-green birefringence as they displayed a maximal peak at 540 nm in the absorbance spectrum in the range of 400-700 nm (Figure 4B). The *b* value was consistent with the ThT fluorescence measurements, indicating major β -aggregation for β 3 and β 7 peptides. Furthermore, all peptide aggregates were examined by TEM to evaluate their morphology. The four peptide aggregates displayed fibrillar morphology; however, a major degree of association was achieved by the β 3 peptide since it formed a dense net of mature fibers (Figure 5).

4.3. Acid hydrolysis of HsTPI.

It is clear that a weak destabilization of the $(\beta/\alpha)_8$ barrel from HsTPI in 3.2 M urea does not allow a complete exposure of the primary structure of HsTPI. Acid treatment of HsTPI

not only denatures their tertiary structure but also hydrolyzes the primary structure at aspartic residues, allowing a complete coverage in the fibrillogenic regions scan^{25,41,42}. The acid hydrolysis of HsTPI was performed at pH 2.0 at 65 °C. After 8 h of incubation, the cleavage products were examined by Tricine SDS-PAGE showing more than 80 % of the total protein hydrolysis, as determined by densitometry using Image LabTM software-BioRad (Figure 6A).

After acid hydrolysis, the reaction mixture was incubated at 37 °C and 600 rpm. The β -aggregation was monitored by ThT fluorescence measurements. The hydrolyzed fragments mixture was aggregated following a nucleated polymerization mechanism with a lag phase, of approximately 45 h and saturation after 140 h (Figure 6B). The TEM images of the final aggregation products further demonstrated its fibrillar morphology (Figure 6C). These results were indicative of amyloid-like fibril formation; however, the residues involved in amyloid fibril formation were unknown.

To determinate what regions of the protein were present in the fibrillar aggregates, this was first thoroughly washed with phosphate buffer to eliminate all soluble fragments. Subsequently, the fibrillar aggregate were partially dissociated overnight with 7.4 M Gdm-HCl. The guanidine-solvated fraction was recovered and visualized by Tricine SDS-PAGE showing mainly one band below the 10 kDa mark (Figure 6D). The nLC-MS/MS analysis showed that only one fragment was incorporated in the fibril. This fragment corresponded to the region comprising residues 57-85 of HsTPI (Figure 6E). This region covers the entire β 3-strand and most of the α 3-helix of the (β/α)₈ barrel. As displayed in the resultant sequence, the glutamine 65 was deaminated into a glutamate due to acid treatment of the protein. However, this chemical change had no effect in fibrillogenic propensity since both,

the synthetic (β 3 peptide) and hydrolyzed fragment, were able to form amyloid-like fibrils. It is noteworthy that despite the fact that every aspartic residue was a potential cleavage site⁴¹ and therefore all predicted segments were potentially covered, no other fragment was aggregated upon hydrolysis.

5. Discussion

5.1 HsTPI aggregation.

The incubation of HsTPI_n led to non-fibrillar aggregates as shown in the TEM images. ATR-FTIR analysis of this aggregates revealed that HsTPI_n aggregates kept most of its native secondary structure. Previous *in vitro* studies have remarked that globular protein can self-assemble into native-like aggregates promoted by subtle conformational changes not necessarily implying unfolding, that can be on- or off-pathway of fibrillogenesis^{43,44}. Aggregation kinetics followed by ThT fluorescence shown no amyloid formation tendency for HsTPI_n after one week of incubation. Hence, HsTPI_n incubation resulted in a rapid native-like aggregation without a further β -aggregation. These results suggest that HsTPI under native-favoring conditions has great stability that prevents β -aggregation. In that matter and similarly to others TPIs studied, HsTPI thermal denaturation follows a two-state irreversible model with a first-order kinetic rate constant of $7.2 \times 10^{-6} \text{ min}^{-1}$ at 37°C ^{45,46}. According to this value, seven days of incubation under native-favoring conditions are insufficient to allow HsTPI to visit conformational states that could lead to fibrillogenesis.

On the other hand, the slightly destabilization of HsTPI structure with 3.2 M of urea²⁹ showed an increase in ThT fluorescence intensities (Figure 1A) suggesting that native state is protected by a high energy barrier that impedes the exploration of intermediate states

leading to β -aggregation. Higher concentrations of urea did not increase β -aggregation (Supporting Information Figure S2), as expected, since urea solvates the protein's main-chain and competes with the hydrogen bonds during β -aggregation⁴⁷⁻⁴⁹. In addition to ThT fluorescence, HsTPI_{urea} aggregates were analyzed by ATR-FTIR demonstrating formation of new β -structure with a characteristic lower-frequency band position around 1624 cm⁻¹ indicative of cross- β formation^{50,51}. Even though, recent studies have sighted a clear tendency in new β -structure formation upon aggregation, despite the nature of the aggregate, the position of the band below 1630 nm is indicative of a stronger H-bond formation as in fibrils^{28,52}. In this regard, cross- β structure was further confirmed by the recognition of WO1 antibody³⁵.

It is interesting to note that destabilized HsTPI did not follow a nucleated polymerization mechanism typical of amyloid formation. Instead, the kinetics showed a non-cooperative monophasic increase with absence of a lag phase. This behavior suggests that HsTPI in 3.2 M of urea is in a conformational state that allows β -aggregation in a nucleated independent mechanism^{5,8}. A similar behavior was observed in the amyloid fibril formation of the SH3 domain of the PI3 kinase, which at pH 3.6 formed amorphous aggregates (1-3 h) with the posterior appearing of curly fibrils (5 days)⁵³. It was suggested in that work, that amorphous aggregates were energetically more favorable than the nucleation needed for fibril formation. It has been described a similar cooperativity in both amorphous and β -sheet oligomerization, suggesting that disorder aggregation could compete with β -aggregation in early steps of fibril formation^{17,54,55}. Furthermore, this early amorphous aggregates can play an important role in the recruitment and association of protein molecules into fibrillar structure by conformational conversion⁵⁶⁻⁵⁸. This proposed

mechanism can explain the co-aggregation of disordered structures with poor fibrillar morphology showed in TEM images of HsTPI_{urea} aggregates, indicating that the fibrillogenesis was on track but it was incomplete after 7 days of incubation.

5.2. Fibrillogenic region of HsTPI.

The identification of fibrillogenic regions was achieved through different algorithms. From these, eight consensus predictions were found, from which, only 3 peptides covering the regions β 6, β 7 and CS-3 formed fibrillar amyloid-like aggregates as confirmed by fluorescence and birefringence assays (Figure 4). In particular, the β -aggregation of the β 7 peptide was consistent with previous evidence of amyloid-like aggregation in the region containing the equivalent strand in the *Escherichia coli* TPI²³. However, Contreras et al., (1999) did not delimit the cross- β core to the 32 residue fragment. According to our results, we can infer that β 7-strand is at least one cross- β core in the *E. coli* TPI fibrillogenic fragment (186–218) due to its high identity with β 7-strand from HsTPI.

It is noteworthy that, in addition to the consensual predicted regions, we found that the sequence comprising the β 3-strand (residues 59-66) was highly fibrillogenic. Only the AMYLPRED 2 server identified the β 3 sequence as fibrillogenic, reflecting better accuracy than the other predictors used³⁸. All others studied peptides showed amorphous aggregation or no aggregation at all. The peptide aggregation analysis confirmed four fibrillogenic regions within HsTPI sequence. However, only 38.9% of protein sequence was evaluated by this approach. In order to cover most of the sequence, fibrillogenesis was further analyzed on aspartic-specific fragmented HsTPI. After partial hydrolysis and incubation, HsTPI fragments were assembled into amyloid-like aggregates. From all fragments available for aggregation, the fragment containing the β 3-strand was the only one

present in the amyloid fibril formed, indicating the high fibrillogenic propensity of that β -strand. Interestingly, the β -aggregation of this hydrolyzed fragment followed a nucleated polymerization mechanism. This observation in contrast with the non-cooperative monophasic transition exhibited by HsTPI_{urea} suggests that competitive interactions, beside the cross- β interaction, lead to an aggregation pathway that delayed the β -aggregation of HsTPI.

5.3. Amyloid protective features in HsTPI.

The presence of at least 4 cross- β cores, including one with high fibrillogenic propensity, in a highly expressed protein that participates in the central metabolism of any living cell, raises the question of how nature has avoided the major catastrophic events that could preclude the necessary balance to sustain life. Some structural characteristics of HsTPI topology could be consider as protective features. First, all parallel β -stands are buried inside the protein, forming a β -barrel that prevents further β -sheet propagation and, thereby, β -aggregation. In order to β -aggregate, the fibrillogenic β -strands found in this study (β 3, β 6 and β 7) must be exposed to the surface. However, because the amino acids constituting the β -barrel are predominantly hydrophobic, the exposure of the inner core may collapse into amorphous aggregates instead of rapidly forming cross- β structures, retarding or avoiding amyloid-like aggregation.

In the case of solvent-exposed regions, which are more accessible for intermolecular associations, there is a structural restriction avoiding the β -conformation that promotes the α -helix or random coil conformations. This mechanism could prevent the cross- β association of CS-3 in the native fold because this region is restricted to the last α -helix of HsTPI.

It is noteworthy that most of the predicted and demonstrated fibrillogenic regions are in the C-terminus half of the protein. Recent studies of *in vivo* folding indicate that folding starts as soon as the polypeptide chain leaves the ribosome tunnel⁵⁹. So that *in vivo*, by the time the C-regions are exposed, the N-terminus half has probably started its folding process, directing the folding of the remaining of the polypeptide, and avoiding any off-pathway intermolecular interaction. Once the native state is reached its high energy barrier protects it from partial unfolding that could expose these regions^{60,61}.

In addition to the tertiary structure of $(\beta/\alpha)_8$, TPI is always found as an oligomer, and more frequently as a dimer. This intermolecular association results in an increase almost 8-fold in the stability of the human enzyme²⁹. The interface region is precisely formed by the loop following the $\beta 3$ -strand that interdigitates into the active site of the other subunit. This interaction gives extra protection to the region around the $\beta 3$ -strand. Although most of the efforts to perturb the dimeric interface of the protein have yielded inactive proteins⁶²⁻⁶⁴, the generation of a sufficiently active monomeric variant⁶⁵ rules out the possibility that activity is the only major selective pressure for this protein to maintain its oligomeric state. Instead, it is possible that the changes in tertiary contacts in the fibrillogenic regions upon dimerization, increases the energetic barrier for the formation of amyloidogenic fibers, as suggested by Buell et al.⁶⁶, which could be another selective factor to maintain TPIs as dimers.

In addition, it has been observed that the size of polypeptide chain could influence in the aggregation of proteins^{13,67,68}. The length of the polypeptide chain could be associated with the number of possible conformation states in the intermolecular protein association increasing the number and complexity of the aggregation pathways. Since HsTPI is a

medium-size protein with a compact, stable and evolution-selected topology is reasonably to speculate the existence of competitive aggregation pathways, once the native state is altered, that avoid cross- β formation.

6. Conclusion

It is clear that albeit containing at least four potential amyloidogenic regions, the nature of HsTPI confers protection against the formation of toxic amyloid aggregates. However, mutations or post-translational modifications might affect its solubility, stability and/or folding, allowing it to develop a role in amyloid diseases.

7. Acknowledgments

We thank Dr. Ronald Wetzel and Ravindra Kodali for kindly donating the WO1 antibody, Dr. Armando Gómez Poyou† for providing the pET3a-HsTPI plasmid, Biol. Filiberto Sanchez López for technical support, and the following facilities of the Instituto de Biotecnología, Universidad Nacional Autónoma de México for their services at different stages of this work: Laboratorio Nacional de Microscopía Avanzada, specifically, Dr. Guadalupe Zavala; Laboratorio Universitario de Proteómica, specifically Dr. Cesar Ferreira Batista; and Unidad de Cómputo and Unidad de Biblioteca. Thanks the Consejo Nacional de Ciencia y Tecnología for the doctoral scholarship. This work was supported by the Programa de Apoyo a Proyectos de Investigación e Innovación Tecnológica (PAPIIT) (grant number IN211414 to G.S.R.) and the Consejo Nacional de Ciencia y Tecnología (CONACYT) (grant number 154194).

7. References

- 1 Chiti, F. & Dobson, C. M. Protein misfolding, functional amyloid, and human disease. *Annual review of biochemistry* **75**, 333-366, doi:10.1146/annurev.biochem.75.101304.123901 (2006).
- 2 Knowles, T. P., Vendruscolo, M. & Dobson, C. M. The amyloid state and its association with protein misfolding diseases. *Nature reviews. Molecular cell biology* **15**, 384-396, doi:10.1038/nrm3810 (2014).
- 3 Westermarck, P. Aspects on human amyloid forms and their fibril polypeptides. *FEBS J* **272**, 5942-5949, doi:10.1111/j.1742-4658.2005.05024.x (2005).
- 4 Jahn, T. R. *et al.* The common architecture of cross-beta amyloid. *Journal of molecular biology* **395**, 717-727, doi:10.1016/j.jmb.2009.09.039 (2010).
- 5 Zerovnik, E. *et al.* Mechanisms of amyloid fibril formation--focus on domain-swapping. *The FEBS journal* **278**, 2263-2282, doi:10.1111/j.1742-4658.2011.08149.x (2011).

- 6 Gillam, J. E. & MacPhee, C. E. Modelling amyloid fibril formation kinetics: mechanisms of nucleation and growth. *Journal of physics. Condensed matter : an Institute of Physics journal* **25**, 373101, doi:10.1088/0953-8984/25/37/373101 (2013).
- 7 Powers, E. T. & Powers, D. L. Mechanisms of protein fibril formation: nucleated polymerization with competing off-pathway aggregation. *Biophysical journal* **94**, 379-391, doi:10.1529/biophysj.107.117168 (2008).
- 8 Dovidchenko, N. V., Leonova, E. I. & Galzitskaya, O. V. Mechanisms of amyloid fibril formation. *Biochemistry. Biokhimiia* **79**, 1515-1527, doi:10.1134/S0006297914130057 (2014).
- 9 Wu, C. & Shea, J. E. Coarse-grained models for protein aggregation. *Current opinion in structural biology* **21**, 209-220, doi:10.1016/j.sbi.2011.02.002 (2011).
- 10 Gosal, W. S. *et al.* Competing pathways determine fibril morphology in the self-assembly of beta2-microglobulin into amyloid. *Journal of molecular biology* **351**, 850-864, doi:10.1016/j.jmb.2005.06.040 (2005).
- 11 Calamai, M., Chiti, F. & Dobson, C. M. Amyloid fibril formation can proceed from different conformations of a partially unfolded protein. *Biophysical journal* **89**, 4201-4210, doi:10.1529/biophysj.105.068726 (2005).
- 12 Zou, Y. *et al.* New insight into amyloid fibril formation of hen egg white lysozyme using a two-step temperature-dependent FTIR approach. *The journal of physical chemistry. B* **118**, 9834-9843, doi:10.1021/jp504201k (2014).
- 13 Baldwin, A. J. *et al.* Metastability of native proteins and the phenomenon of amyloid formation. *J Am Chem Soc* **133**, 14160-14163, doi:10.1021/ja2017703 (2011).
- 14 Jahn, T. R. & Radford, S. E. Folding versus aggregation: polypeptide conformations on competing pathways. *Archives of biochemistry and biophysics* **469**, 100-117, doi:10.1016/j.abb.2007.05.015 (2008).
- 15 Maurer-Stroh, S. *et al.* Exploring the sequence determinants of amyloid structure using position-specific scoring matrices. *Nature methods* **7**, 237-242, doi:10.1038/nmeth.1432 (2010).
- 16 Fernandez-Escamilla, A. M., Rousseau, F., Schymkowitz, J. & Serrano, L. Prediction of sequence-dependent and mutational effects on the aggregation of peptides and proteins. *Nature biotechnology* **22**, 1302-1306, doi:10.1038/nbt1012 (2004).
- 17 Hills, R. D., Jr. & Brooks, C. L., 3rd. Hydrophobic cooperativity as a mechanism for amyloid nucleation. *Journal of molecular biology* **368**, 894-901, doi:10.1016/j.jmb.2007.02.043 (2007).
- 18 Tzotzos, S. & Doig, A. J. Amyloidogenic sequences in native protein structures. *Protein science : a publication of the Protein Society* **19**, 327-348, doi:10.1002/pro.314 (2010).
- 19 Richardson, J. S. & Richardson, D. C. Natural beta-sheet proteins use negative design to avoid edge-to-edge aggregation. *Proc Natl Acad Sci U S A* **99**, 2754-2759, doi:10.1073/pnas.052706099 (2002).
- 20 Goldstein, R. A. The structure of protein evolution and the evolution of protein structure. *Current opinion in structural biology* **18**, 170-177, doi:<http://dx.doi.org/10.1016/j.sbi.2008.01.006> (2008).
- 21 Koehl, P. & Levitt, M. Protein topology and stability define the space of allowed sequences. *Proc Natl Acad Sci U S A* **99**, 1280-1285, doi:10.1073/pnas.032405199 (2002).
- 22 Wierenga, R. K. The TIM-barrel fold: a versatile framework for efficient enzymes. *FEBS Letters* **492**, 193-198, doi:[http://dx.doi.org/10.1016/S0014-5793\(01\)02236-0](http://dx.doi.org/10.1016/S0014-5793(01)02236-0) (2001).
- 23 Contreras, C. F., Canales, M. A., Alvarez, A., De Ferrari, G. V. & Inestrosa, N. C. Molecular modeling of the amyloid-beta-peptide using the homology to a fragment of triosephosphate isomerase that forms amyloid in vitro. *Protein engineering* **12**, 959-966 (1999).

- 24 Guix, F. X. *et al.* Amyloid-dependent triosephosphate isomerase nitrotyrosination induces glycation and tau fibrillation. *Brain* **132**, 1335-1345 (2009).
- 25 Mishra, R. *et al.* Lysozyme amyloidogenesis is accelerated by specific nicking and fragmentation but decelerated by intact protein binding and conversion. *Journal of molecular biology* **366**, 1029-1044, doi:10.1016/j.jmb.2006.11.084 (2007).
- 26 Klunk, W. E., Jacob, R. F. & Mason, R. P. Quantifying amyloid beta-peptide (Abeta) aggregation using the Congo red-Abeta (CR-abeta) spectrophotometric assay. *Anal Biochem* **266**, 66-76, doi:S0003-2697(98)92933-5 [pii] 10.1006/abio.1998.2933 (1999).
- 27 Frid, P., Anisimov, S. V. & Popovic, N. Congo red and protein aggregation in neurodegenerative diseases. *Brain research reviews* **53**, 135-160, doi:10.1016/j.brainresrev.2006.08.001 (2007).
- 28 Shivu, B. *et al.* Distinct beta-sheet structure in protein aggregates determined by ATR-FTIR spectroscopy. *Biochemistry* **52**, 5176-5183, doi:10.1021/bi400625v (2013).
- 29 Mainfroid, V., Mande, S. C., Hol, W. G., Martial, J. A. & Goraj, K. Stabilization of human triosephosphate isomerase by improvement of the stability of individual alpha-helices in dimeric as well as monomeric forms of the protein. *Biochemistry* **35**, 4110-4117, doi:10.1021/bi952692n (1996).
- 30 Mainfroid, V. *et al.* Three hTIM mutants that provide new insights on why TIM is a dimer. *Journal of molecular biology* **257**, 441-456, doi:10.1006/jmbi.1996.0174 (1996).
- 31 Dong, A., Huang, P. & Caughey, W. S. Protein secondary structures in water from second-derivative amide I infrared spectra. *Biochemistry* **29**, 3303-3308 (1990).
- 32 Baldassarre, M., Scire, A., Fiume, I. & Tanfani, F. Insights into the structural properties of D-serine dehydratase from *Saccharomyces cerevisiae*: an FT-IR spectroscopic and in silico approach. *Biochimie* **93**, 542-548, doi:10.1016/j.biochi.2010.11.009 (2011).
- 33 Kong, J. & Yu, S. Fourier transform infrared spectroscopic analysis of protein secondary structures. *Acta biochimica et biophysica Sinica* **39**, 549-559 (2007).
- 34 Huang, P. & Dong, A. Thermal, chemical and chemothermal denaturation of yeast enolase. *Spectroscopy* **17**, doi:10.1155/2003/941801 (2003).
- 35 O'Nuallain, B. & Wetzel, R. Conformational Abs recognizing a generic amyloid fibril epitope. *Proc Natl Acad Sci U S A* **99**, 1485-1490, doi:10.1073/pnas.022662599 (2002).
- 36 Gasior, P. & Kotulska, M. FISH Amyloid - a new method for finding amyloidogenic segments in proteins based on site specific co-occurrence of aminoacids. *BMC bioinformatics* **15**, 54, doi:10.1186/1471-2105-15-54 (2014).
- 37 Garbuzynskiy, S. O., Lobanov, M. Y. & Galzitskaya, O. V. FoldAmyloid: a method of prediction of amyloidogenic regions from protein sequence. *Bioinformatics* **26**, 326-332, doi:10.1093/bioinformatics/btp691 (2010).
- 38 Tsolis, A. C., Papandreou, N. C., Iconomidou, V. A. & Hamodrakas, S. J. A consensus method for the prediction of 'aggregation-prone' peptides in globular proteins. *PloS one* **8**, e54175, doi:10.1371/journal.pone.0054175 (2013).
- 39 Walsh, I., Seno, F., Tosatto, S. C. & Trovato, A. PASTA 2.0: an improved server for protein aggregation prediction. *Nucleic Acids Res*, doi:10.1093/nar/gku399 (2014).
- 40 Nilsson, M. R. Techniques to study amyloid fibril formation in vitro. *Methods* **34**, 151-160, doi:10.1016/j.ymeth.2004.03.012 (2004).
- 41 Li, A. *et al.* Chemical cleavage at aspartyl residues for protein identification. *Anal Chem* **73**, 5395-5402 (2001).
- 42 Fink, A. L., Calciano, L. J., Goto, Y., Kurotsu, T. & Palleros, D. R. Classification of acid denaturation of proteins: intermediates and unfolded states. *Biochemistry* **33**, 12504-12511 (1994).
- 43 Bemporad, F. & Chiti, F. "Native-like aggregation" of the acylphosphatase from *Sulfolobus solfataricus* and its biological implications. *FEBS Letters* **583**, 2630-2638, doi:<http://dx.doi.org/10.1016/j.febslet.2009.07.013> (2009).

- 537 44 Jahn, T. R., Parker, M. J., Homans, S. W. & Radford, S. E. Amyloid formation under
538 physiological conditions proceeds via a native-like folding intermediate. *Nature structural*
539 *& molecular biology* **13**, 195-201, doi:10.1038/nsmb1058 (2006).
- 540 45 Costas, M. *et al.* Between-species variation in the kinetic stability of TIM proteins linked to
541 solvation-barrier free energies. *Journal of molecular biology* **385**, 924-937,
542 doi:10.1016/j.jmb.2008.10.056 (2009).
- 543 46 Aguirre, Y. *et al.* Different contribution of conserved amino acids to the global properties
544 of triosephosphate isomerases. *Proteins* **82**, 323-335, doi:10.1002/prot.24398 (2014).
- 545 47 Zhang, X., Dong, Y., Yu, J. & Tu, X. Effects of environmental factors on MSP21-25
546 aggregation indicate the roles of hydrophobic and electrostatic interactions in the
547 aggregation process. *European biophysics journal : EBJ* **43**, 1-9, doi:10.1007/s00249-013-
548 0934-9 (2014).
- 549 48 Cai, Z. *et al.* Effect of urea concentration on aggregation of amyloidogenic hexapeptides
550 (NFGAIL). *The journal of physical chemistry. B* **118**, 48-57, doi:10.1021/jp407776e
551 (2014).
- 552 49 Hamada, D. & Dobson, C. M. A kinetic study of beta-lactoglobulin amyloid fibril
553 formation promoted by urea. *Protein science : a publication of the Protein Society* **11**,
554 2417-2426, doi:10.1110/ps.0217702 (2002).
- 555 50 Zandomenighi, G., Krebs, M. R. H., McCammon, M. G. & Fändrich, M. FTIR reveals
556 structural differences between native β -sheet proteins and amyloid fibrils. *Protein science :*
557 *a publication of the Protein Society* **13**, 3314-3321, doi:10.1110/ps.041024904 (2004).
- 558 51 Moran, S. D. & Zanni, M. T. How to Get Insight into Amyloid Structure and Formation
559 from Infrared Spectroscopy. *The Journal of Physical Chemistry Letters* **5**, 1984-1993,
560 doi:10.1021/jz500794d (2014).
- 561 52 Wang, L., Schubert, D., Sawaya, M. R., Eisenberg, D. & Riek, R. Multidimensional
562 structure-activity relationship of a protein in its aggregated states. *Angewandte Chemie* **49**,
563 3904-3908, doi:10.1002/anie.201000068 (2010).
- 564 53 Bader, R., Bamford, R., Zurdo, J., Luisi, B. F. & Dobson, C. M. Probing the mechanism of
565 amyloidogenesis through a tandem repeat of the PI3-SH3 domain suggests a generic model
566 for protein aggregation and fibril formation. *Journal of molecular biology* **356**, 189-208,
567 doi:10.1016/j.jmb.2005.11.034 (2006).
- 568 54 Vetri, V. *et al.* Amyloid fibrils formation and amorphous aggregation in concanavalin A.
569 *Biophysical chemistry* **125**, 184-190, doi:10.1016/j.bpc.2006.07.012 (2007).
- 570 55 Krishnan, S. & Raibekas, A. A. Multistep aggregation pathway of human interleukin-1
571 receptor antagonist: kinetic, structural, and morphological characterization. *Biophysical*
572 *journal* **96**, 199-208, doi:10.1016/j.bpj.2008.10.002 (2009).
- 573 56 Auer, S., Meersman, F., Dobson, C. M. & Vendruscolo, M. A generic mechanism of
574 emergence of amyloid protofilaments from disordered oligomeric aggregates. *PLoS*
575 *computational biology* **4**, e1000222, doi:10.1371/journal.pcbi.1000222 (2008).
- 576 57 Serio, T. R. *et al.* Nucleated conformational conversion and the replication of
577 conformational information by a prion determinant. *Science* **289**, 1317-1321 (2000).
- 578 58 Johnson, S. M., Connelly, S., Fearn, C., Powers, E. T. & Kelly, J. W. The transthyretin
579 amyloidosis: from delineating the molecular mechanism of aggregation linked to pathology
580 to a regulatory-agency-approved drug. *Journal of molecular biology* **421**, 185-203,
581 doi:10.1016/j.jmb.2011.12.060 (2012).
- 582 59 O'Brien, E. P., Hsu, S. T., Christodoulou, J., Vendruscolo, M. & Dobson, C. M. Transient
583 tertiary structure formation within the ribosome exit port. *J Am Chem Soc* **132**, 16928-
584 16937, doi:10.1021/ja106530y (2010).
- 585 60 Ugrinov, K. G. & Clark, P. L. Cotranslational folding increases GFP folding yield.
586 *Biophysical journal* **98**, 1312-1320, doi:10.1016/j.bpj.2009.12.4291 (2010).

587 61 O'Brien, E. P., Christodoulou, J., Vendruscolo, M. & Dobson, C. M. New scenarios of
588 protein folding can occur on the ribosome. *J Am Chem Soc* **133**, 513-526,
589 doi:10.1021/ja107863z (2011).

590 62 Borchert, T. V., Abagyan, R., Jaenicke, R. & Wierenga, R. K. Design, creation, and
591 characterization of a stable, monomeric triosephosphate isomerase. *Proc Natl Acad Sci U S*
592 *A* **91**, 1515-1518 (1994).

593 63 Borchert, T. V. *et al.* An interface point-mutation variant of triosephosphate isomerase is
594 compactly folded and monomeric at low protein concentrations. *Febs Lett* **367**, 315-318
595 (1995).

596 64 Schliebs, W., Thanki, N., Jaenicke, R. & Wierenga, R. K. A double mutation at the tip of
597 the dimer interface loop of triosephosphate isomerase generates active monomers with
598 reduced stability. *Biochemistry* **36**, 9655-9662 (1997).

599 65 Saab-Rincon, G., Juarez, V. R., Osuna, J., Sanchez, F. & Soberon, X. Different strategies to
600 recover the activity of monomeric triosephosphate isomerase by directed evolution. *Protein*
601 *engineering* **14**, 149-155 (2001).

602 66 Buell, A. K. *et al.* Detailed analysis of the energy barriers for amyloid fibril growth.
603 *Angewandte Chemie* **51**, 5247-5251 (2012).

604 67 Solomon, J. P. *et al.* The 8 and 5 kDa Fragments of Plasma Gelsolin Form Amyloid Fibrils
605 by a Nucleated Polymerization Mechanism, while the 68 kDa Fragment is Not
606 Amyloidogenic. *Biochemistry* **48**, 11370-11380, doi:10.1021/bi901368e (2009).

607 68 Ramshini, H. *et al.* Large proteins have a great tendency to aggregate but a low propensity
608 to form amyloid fibrils. *PloS one* **6**, e16075, doi:10.1371/journal.pone.0016075 (2011).

609

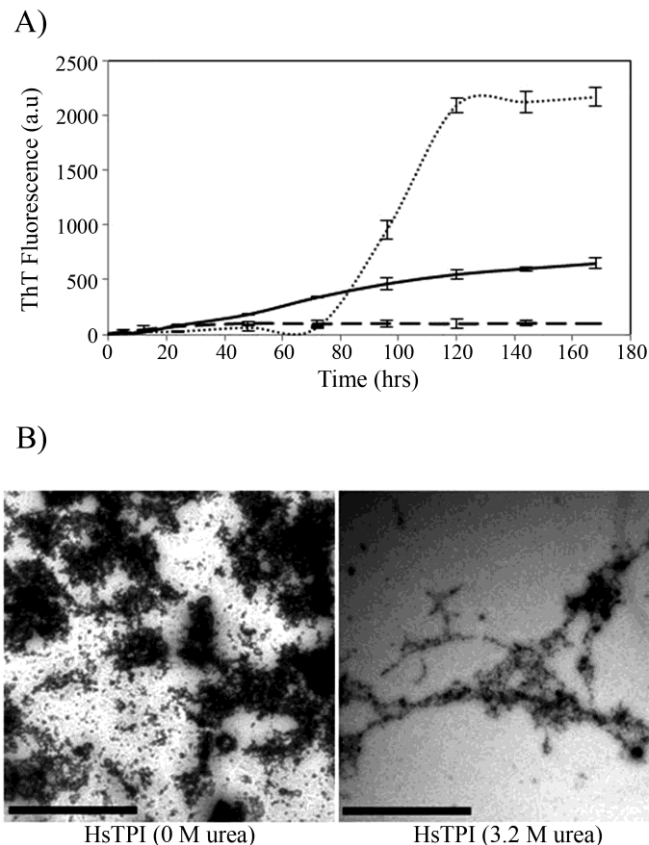


Figure 1. HsTPI aggregation. A) Aggregation kinetics followed by ThT fluorescence showing a slow β -aggregation of HsTPI under partially unfolding conditions (3.2 M of urea) (solid line) and practical non under native-like conditions (dashed line). HEWL (dotted line) was used as the positive control of fibril formation. B) TEM images of HsTPI aggregates at the final time point of aggregation. Scale bars are 1 μ M.

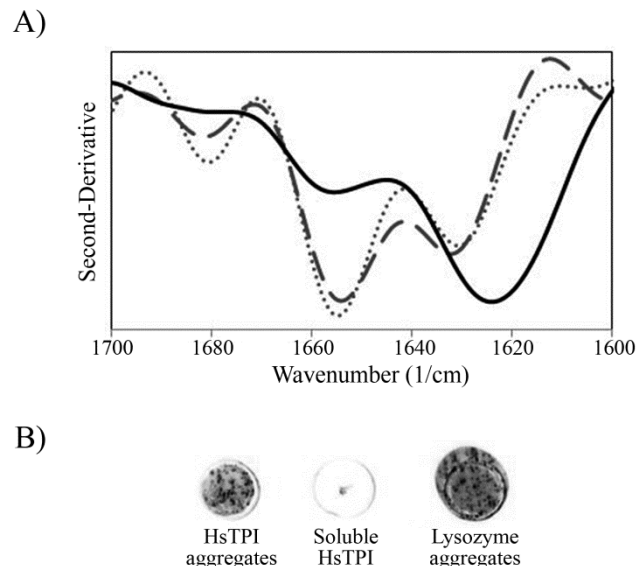


Figure 2. Secondary structure of HsTPI aggregates. A) Second-derivative ATF-FTIR spectra in the amide I region. After incubation, second structure of HsTPI was practically unchanged under native-like condition (dashed line) compared with the salted-out HsTPI (dotted line). However HsTPI aggregated in 3.2 M of urea (solid line) showed a shift in the β -sheet signal to a lower-frequency band from 1633 to 1624 cm^{-1} indicative of β -aggregation and a loss of α -helix around 1655 cm^{-1} . B) Dot-blot assay of HsTPI aggregates with the WO1 antibody confirming cross- β structure.

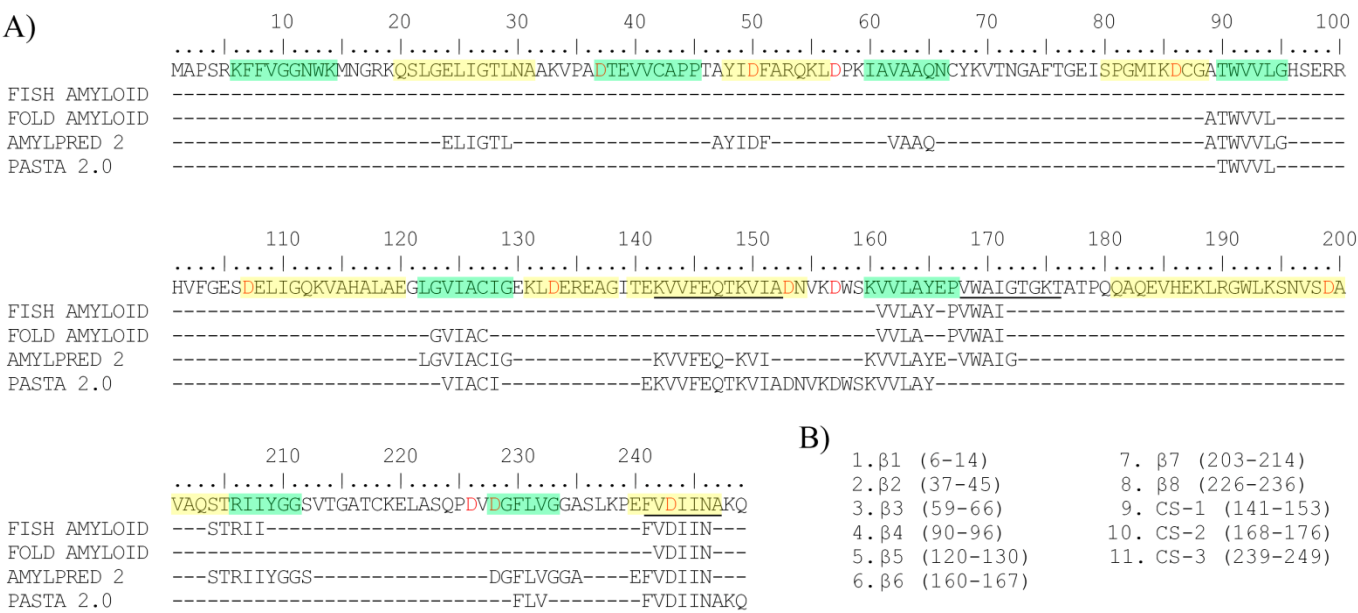
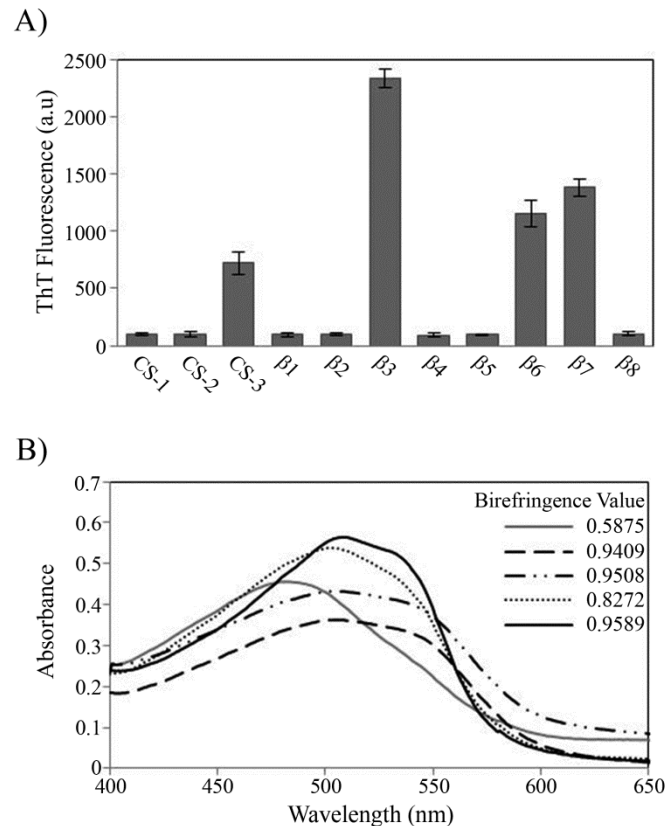


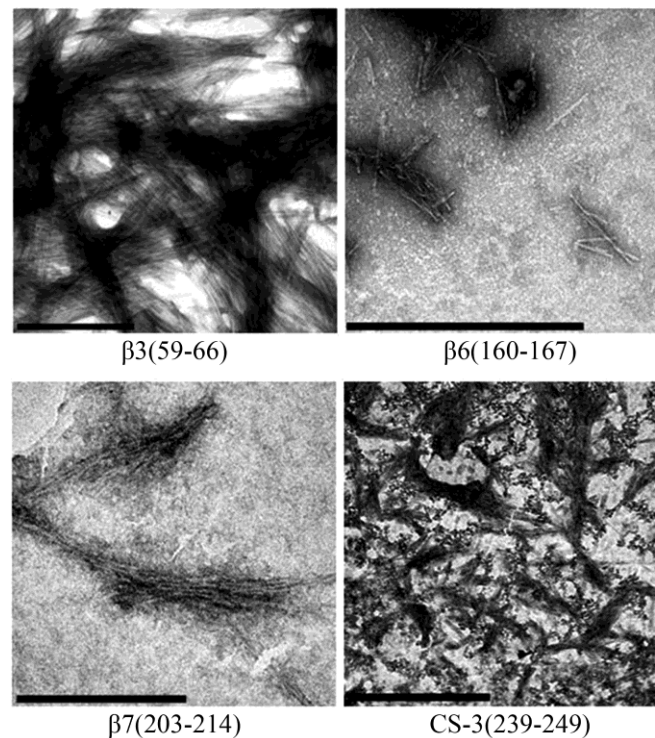
Figure 3. Identification of potential fibrillogenic regions in HsTPI. A) Consensus amyloid formation predictions in HsTPI. The β -strands are shown in green, the α -helices in yellow and the chameleonic sequences are underlined. Aspartic residues are in red, indicating the potential acid hydrolysis sites. Hits are shown in corresponding line to the predictor. B) List of the potential fibrillogenic regions selected for peptide aggregation assay. All β -strand were selected as well as the three more significant chameleonic sequences in the protein.



636

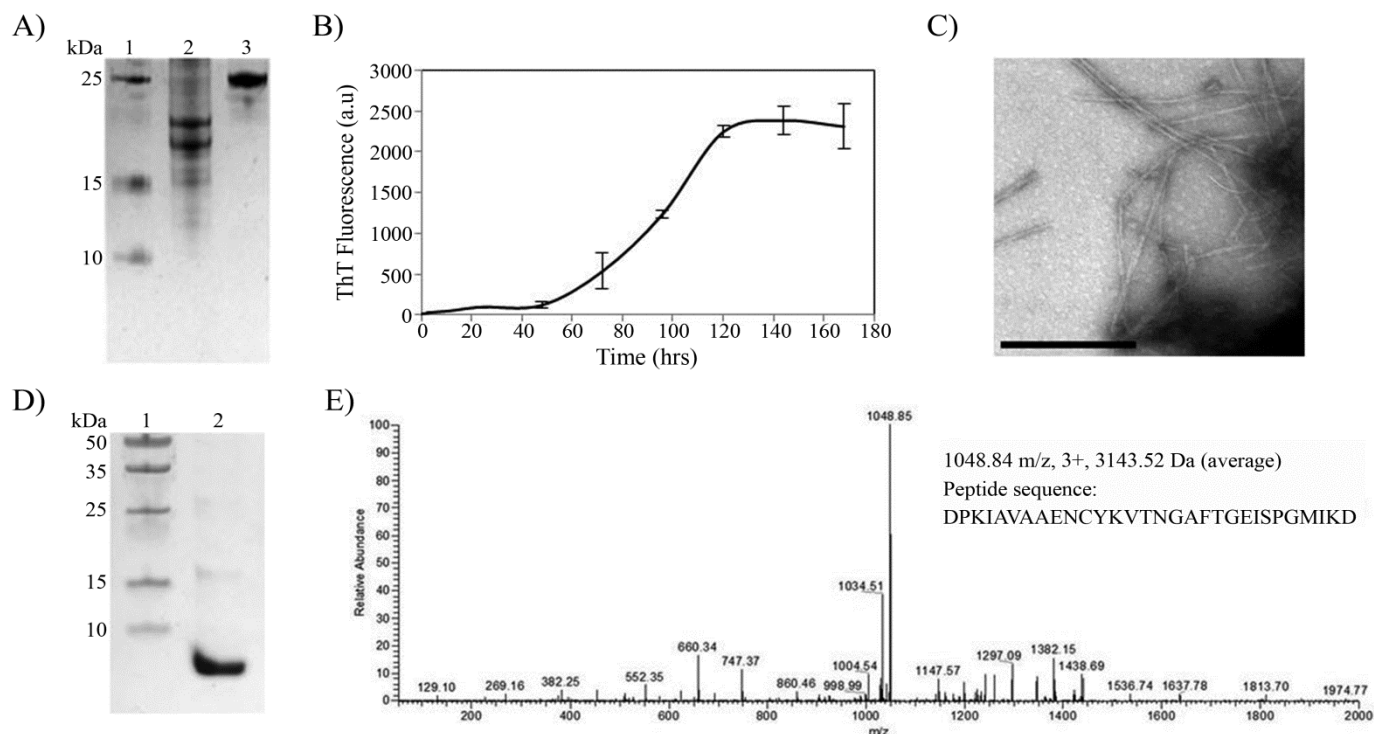
637 **Figure 4.** Peptides aggregation. A) ThT fluorescence intensities at 485 nm of potential
 638 fibrillogenic peptides after 3 week of aggregation. Only four peptides formed β -aggregates
 639 (β_3 , β_6 , β_7 and CS-3 peptide) indicated with an increase in ThT fluorescence intensity. B)
 640 Congo red birefringence assay of the β_3 (solid black line), β_6 (dashed line), β_7 -peptide
 641 (dotted-dashed line) and CS-3-peptide (dotted line) aggregates. A maximal peak at 540 nm
 642 is shown in aggregates compared with Congo red alone (solid gray line).

643



644

645 **Figure 5.** TEM images of peptides aggregates. Different morphologies were displayed by
 646 the peptide aggregates; $\beta 3$ peptide formed a dense net of highly associated fibrils while $\beta 6$
 647 and $\beta 7$ aggregates shown poor fibril elongation. CS-3 peptide was co-aggregated into
 648 fibrillar and disordered aggregates. The scale bar is 1 μm .



649

Figure 6. Fibrillogenic behavior of chemically cleaved HsTPI. A) SDS-PAGE of acid hydrolyzed HsTPI. Lane 1 shows the protein molecular weight marker as indicated; lane 2, the products of acid hydrolysis of HsTPI and lane 3, HsTPI before the reaction. B) Aggregation kinetics of the products of HsTPI acid hydrolysis followed by ThT fluorescence. C) TEM image of the amyloid fibrils formed by the HsTPI hydrolysis products; the scale bars is 1 μ M. D) Tricine SDS-PAGE of the enriched fragment upon aggregation. E) MS/MS spectrum of the triply charged precursor ion at m/z 1048.84 identifies the amyloid fragment as the sequence DPKIAVAAENCYKVTNGAFTGEISPGMIKD, which corresponds to residues 57-85 of HsTPI.